



## OPEN ACCESS

EDITED BY  
Gilles Reverdin,  
Centre National de la Recherche  
Scientifique (CNRS), France

REVIEWED BY  
Wei-dong Zhai,  
Shandong University, China  
Andrea Pain,  
University of Maryland, College Park,  
United States

\*CORRESPONDENCE  
Daiki Nomura  
daiki.nomura@fish.hokudai.ac.jp

SPECIALTY SECTION  
This article was submitted to  
Marine Biogeochemistry,  
a section of the journal  
Frontiers in Marine Science

RECEIVED 11 February 2022

ACCEPTED 29 June 2022

PUBLISHED 22 July 2022

CITATION  
Horikawa T, Nomura D, Kanna N,  
Fukamachi Y and Sugiyama S (2022)  
Effects of the glacial meltwater supply  
on carbonate chemistry in Bowdoin  
Fjord, Northwestern Greenland.  
*Front. Mar. Sci.* 9:873860.  
doi: 10.3389/fmars.2022.873860

COPYRIGHT  
© 2022 Horikawa, Nomura, Kanna,  
Fukamachi and Sugiyama. This is an  
open-access article distributed under  
the terms of the [Creative Commons  
Attribution License \(CC BY\)](https://creativecommons.org/licenses/by/4.0/). The use,  
distribution or reproduction in other  
forums is permitted, provided the  
original author(s) and the copyright  
owner(s) are credited and that the  
original publication in this journal is  
cited, in accordance with accepted  
academic practice. No use,  
distribution or reproduction is  
permitted which does not comply with  
these terms.

# Effects of the glacial meltwater supply on carbonate chemistry in Bowdoin Fjord, Northwestern Greenland

Takahito Horikawa<sup>1</sup>, Daiki Nomura<sup>1,2,3\*</sup>, Naoya Kanna<sup>4</sup>,  
Yasushi Fukamachi<sup>3</sup> and Shin Sugiyama<sup>3,5</sup>

<sup>1</sup>Faculty of Fisheries Sciences, Hokkaido University, Hakodate, Japan, <sup>2</sup>Field Science Center for Northern Biosphere, Hokkaido University, Hakodate, Japan, <sup>3</sup>Arctic Research Center, Hokkaido University, Sapporo, Japan, <sup>4</sup>Atmosphere and Ocean Research Institute, The University of Tokyo, Kashiwa, Japan, <sup>5</sup>Institute of Low Temperature Science, Hokkaido University, Sapporo, Japan

To understand the effects of the glacial meltwater supply on carbonate chemistry and the air–sea CO<sub>2</sub> flux within the fjord, water samples were collected in Bowdoin Fjord in northwestern Greenland for dissolved inorganic carbon (DIC) concentration, total alkalinity (TA), oxygen isotopic ratio ( $\delta^{18}\text{O}$ ), and chlorophyll *a* concentration analyses in the summers of 2016 and 2017. The partial pressure of CO<sub>2</sub> ( $p\text{CO}_2$ ) in surface water, calculated from DIC and TA, was less than 200  $\mu\text{atm}$ , and was significantly lower than that in the atmosphere ( $399 \pm 3 \mu\text{atm}$ ). Therefore, surface water of the fjord acts as sink for CO<sub>2</sub> in the atmosphere ( $-4.9 \pm 0.7 \text{ mmol m}^{-2} \text{ d}^{-1}$ ). To evaluate the effects of freshwater and land-derived substances by glacial meltwater on  $p\text{CO}_2$  in the fjord, we calculated the changes of  $p\text{CO}_2$  in salinity and carbonate chemistry that would result from the inflow of glacial meltwater into the fjord. The calculated  $p\text{CO}_2$  was high near the calving front, where the contribution of glacier meltwater was significant. Examination of the relationship between salinity-normalized DIC and TA, which was considered DIC and TA input from the land, suggested that the land-derived high  $p\text{CO}_2$  freshwater affected mainly by the remineralization of the organic matter by bacterial activity was supplied to the Bowdoin Fjord.

## KEYWORDS

carbonate chemistry, freshwater, fjord, glacier, Greenland

## Introduction

At present, the carbon dioxide (CO<sub>2</sub>) concentration in the Earth's atmosphere is increasing, and both the atmosphere and the ocean are warming. The Arctic Ocean accounts for about 5–14% of the global ocean CO<sub>2</sub> absorption from the atmosphere (Bates and Mathis, 2009). Although the carbon dynamics in basin areas of the Arctic have been well studied (e.g., Bates and Mathis, 2009; Gao et al., 2012), few studies have focused on high-latitude coastal areas such as the Greenland coastal fjord area. When melting occurs in summer, a large amount of meltwater from the Greenland ice sheet and peripheral glaciers flows into fjords around Greenland (Chu, 2014). This glacial meltwater is freshwater, which has a significant impact on physical, chemical, and biological processes in fjord seawater (e.g., Meire et al., 2015; Arrigo et al., 2017). Currently, meltwater is increasing in Greenland under the influence of enhanced warming in the Arctic (Carr et al., 2017; Nienow et al., 2017). Therefore, it is important to increase our understanding of the effects of glacial meltwater on carbon dynamics in seawater.

The dissolved inorganic carbon concentration (DIC) represents the sum of dissolved CO<sub>2</sub> and carbonic acid substances in the ocean, and total alkalinity (TA) is an indicator of the form in which CO<sub>2</sub> exists in seawater. Glacial meltwater reduces the concentrations of these marine carbonate chemistry components through dilution. As a result, the partial pressure of CO<sub>2</sub> (*p*CO<sub>2</sub>) in seawater, which is determined by DIC and TA, is decreased and the ocean can more easily absorb CO<sub>2</sub> from the atmosphere. For example, (Meire et al. 2015; 2017) reported that in Godthåbsfjord, southwestern Greenland, surface water *p*CO<sub>2</sub> is reduced by the supply of glacial meltwater. Moreover, Seifert et al. (2019) showed that waters in the inner part of Nordvestfjord (Scoresby Sound, eastern Greenland), which are more affected by glacial meltwater, have higher biological productivity and higher carbon fixation capacity than waters at the fjord entrance.

If glacial meltwater consisted of pure freshwater (without impurities), then the supply of glacial meltwater to the ocean would simply dilute DIC and TA; however, actual meltwaters flowing into the ocean are turbid, owing to the presence of suspended terrestrial materials. For example, St Pierre et al. (2019) showed that when land-derived minerals (carbonates and silicates) are dissolved in glacial meltwater, CO<sub>2</sub> in the water is consumed, with the result that *p*CO<sub>2</sub> is decreased. Similarly, Sejr et al. (2011) showed that in summer, *p*CO<sub>2</sub> is reduced in Young Sound, northeastern Greenland, as a result of carbonate dissolution and strong stratification caused by the supply of glacial and sea ice melt to the fjord. Furthermore, Fransson et al. (2015) observed calcite and dolomite crystals in glacial ice on Spitsbergen, Svalbard archipelago, and suggested that carbonate-rich glacial meltwater is supplied to the fjords there. Glacial meltwater flowing into fjord also contains organic particles (Kanna et al., 2018). When these organic particles are

remineralized by bacterial activity (respiration), *p*CO<sub>2</sub> increases (Zeebe and Wolf-Gladrow, 2001). Therefore, understanding inorganic carbon dynamics in such coastal fjord waters requires consideration of not only the dilution effect of glacial meltwater but also its effect on CO<sub>2</sub> by biogeochemical processes.

Glacial meltwater not only reduces *p*CO<sub>2</sub> through dilution but also through its effect on primary production in the surface ocean, because the meltwater supplies nutrients in terrestrial materials to the ocean (e.g., Meire et al., 2017; Kanna et al., 2018; Kanna et al., 2020). Meire et al. (2017) reported that in Godthåbsfjord, southwestern Greenland, where glacial meltwater is released from the glacier bed to the bottom of the ocean, the resulting upwelling carries deep seawater rich in nutrients to the surface. As a result, phytoplankton productivity is increased and *p*CO<sub>2</sub> in the surface layer is reduced. In addition, Arrigo et al. (2017) showed that the release of large amounts of meltwater from the Greenland ice sheet in summer supplies abundant nutrients not only to waters of local fjords but also to the open ocean, where they increase phytoplankton production. As a result, open ocean areas near Greenland also act as a sink for atmospheric CO<sub>2</sub> in summer.

The target area of our study was Bowdoin Fjord, northwestern Greenland, which is usually covered by sea ice during June; in early July the ice begins to melt, and it disappears by the end of July (Sugiyama et al., 2015; Kanna et al., 2018; Sugiyama et al., 2021). Waters of both Arctic and Atlantic origin are distributed in the fjord, and glacial and sea ice meltwaters also flow into the fjord (Ohashi et al., 2020). Two glaciers terminate near the innermost part of Bowdoin Fjord; Bowdoin Glacier is a marine-terminating outlet glacier, and Tugto Glacier is a land-terminating glacier (Figure 1). Meltwater from Bowdoin Glacier is released from the glacier bed to the bottom of the fjord. As a result, an extremely turbid plume can be observed in the surface layer near the glacier where the meltwater containing land-derived sediments upwells (Kanna et al., 2018). This upwelling brings deep ocean nutrients and glacier-derived iron-rich water to the surface, causing the activity of phytoplankton, zooplankton, and seabirds to be increased in the plume compared with that in nearby waters (Kanna et al., 2018; Naito et al., 2019; Nishizawa et al., 2019; Kanna et al., 2020). In contrast, meltwater from Tugto Glacier reaches the ocean *via* proglacial streams such that the meltwater and the land-derived sediments are discharged directly into the surface ocean. Thus, rather than being pure freshwater, glacial meltwaters in Bowdoin Fjord are turbid. The presence of dissolved terrestrial minerals (carbonates and silicates) and organic matter in the meltwater complicate the CO<sub>2</sub> dynamics in the fjord. Furthermore, because the *p*CO<sub>2</sub> in surface water is one of the important parameters that determine the amount of CO<sub>2</sub> that is exchanged between the atmosphere and ocean, it is important to evaluate how freshwater dilution, terrestrial materials, and biological production affect the *p*CO<sub>2</sub> dynamics of fjord waters.

The purpose of this study was to clarify the relationship between the inflow of glacial meltwater and the marine

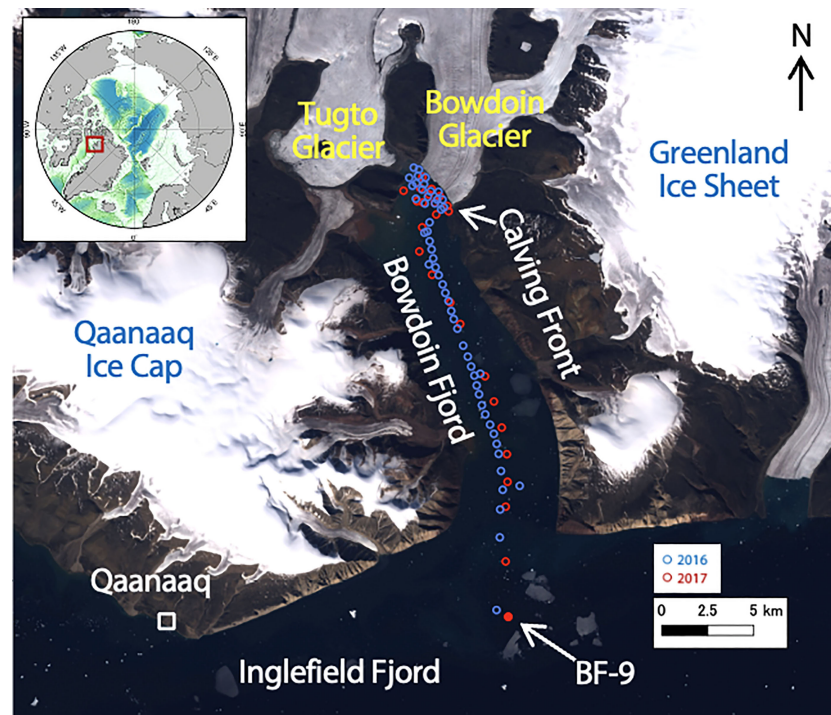


FIGURE 1

Sampling points in Bowdoin Fjord in northwestern Greenland. The Landsat image used for this figure was acquired on 30 July 2016. Blue and red dots indicate sampling points in 2016 and 2017, respectively.

carbonate chemistry in Bowdoin Fjord, especially in surface waters, by analyses of salinity, temperature, DIC, TA, stable oxygen isotope ratios ( $\delta^{18}\text{O}$ ), chlorophyll *a* concentrations (chl.*a*), and  $p\text{CO}_2$ . To this end, we (1) evaluated the relationships between salinity and DIC, TA, and  $p\text{CO}_2$ , (2) clarified the water mass structure of the ocean surface, and (3) evaluated the  $p\text{CO}_2$  dynamics of the surface water, based on the relationship between DIC and TA and the effects of the dissolution of mineral particles, the remineralization by bacterial activity, and primary production. We expect the results of these analyses to facilitate prediction of future changes in the carbonate chemistry of the fjord, and thus the amount of  $\text{CO}_2$  absorbed from the atmosphere, as a result of accelerated melting of the Greenland ice sheet and glaciers.

## Materials and methods

### Observation sites

Field observations were conducted on Bowdoin Glacier and in Bowdoin Fjord between the 7th and 29th of July in 2016 and between the 24th of July and the 1st of August in 2017

(Figure 1). Bowdoin Glacier (Kangerluarsuup Sermia in Greenlandic; Bjørk et al., 2015) is a marine-terminating outlet glacier in northwestern Greenland that discharges freshwater into Bowdoin Fjord along a 3-km-wide calving front. The ice thickness is approximately 250–400 m within 6 km of the terminus, and 86–89% of the entire ice thickness at the terminus is situated below sea level (Sugiyama et al., 2015). The glacier terminus is grounded (Sugiyama et al., 2015); hence, it is not likely to have a floating tongue. Tugto Glacier, a 4-km-wide land-terminating glacier, is several kilometers west of Bowdoin Glacier (Tsutaki et al., 2016), and its proglacial stream discharges freshwater into the fjord. Bowdoin Fjord is approximately 20 km long and is typically covered by sea ice from around October until early July. During our study period, a persistent patch of sediment-rich water was observed on the fjord surface in front of Bowdoin Glacier. We interpreted this patch to be a plume of turbid water that visibly rises toward the fjord surface near the calving front of the glacier. This highly turbid patch is maintained free of sea ice by the upwelling subglacial discharge (Kanna et al., 2018; Podolskiy et al., 2021). In the summers of 2016 and 2017, sea ice began retreating from the fjord in mid-July and had disappeared by the end of July.

## Sampling

We sampled surface fjord water and collected hydrographic data from a 5-m-long boat from within 1 km of the calving front of Bowdoin Glacier to the outer part of Bowdoin Fjord (Figure 1). Sampling point coordinates, time (UTC), and tide information are available in the supporting information as Dataset S1. A conductivity-temperature-depth (CTD) profiler (model ASTD 102, JFE Advantech, Japan) mounted on a pole and suspended from the side of the boat was used to perform continuous measurements of temperature and salinity in the surface waters (0.3 m depth). We took water samples as short a time as possible (generally within 4 hours) to avoid the diurnal variation.

Additionally, surface water samples were collected at 0.3 m depth from the boat into (1) a 120-mL crimp top septum glass bottle (Maruemu Co., Ltd., Osaka, Japan) for measurement of DIC and TA, (2) a 15-mL glass screw-cap vial (Nichiden-Rika Glass Co., Ltd, Kobe, Japan) for measurement of  $\delta^{18}\text{O}$ , (3) a 250-mL glass bottle (Rigo Co., Ltd., Tokyo, Japan) for measurement of salinity, and (4) a 2-L high-density polyethylene bottle (AS ONE, Japan) for measurement of chl.*a*. Surface water samples were also collected from the plume near the glacier front by using a fishing rod and string to lower 500-mL polycarbonate bottles into the water (Kanna et al., 2018), and, subsampled into each bottle. Immediately after subsampling for DIC and TA, a 6.0% (wt.) mercuric chloride ( $\text{HgCl}_2$ ) solution (100  $\mu\text{L}$ ) was added to the samples for DIC and TA to stop biological activity.

Vertical fjord water sampling and hydrographic data collection were also conducted at St. BF-9 (68.465°N, 77.468°W) (Figure 1). The same CTD profiler used for the deep measurement was hung from a Kevlar rope and lowered into the water to measure the water properties every 1 s (~1-m intervals). Fjord water was also sampled at 300 m depth with a Niskin sampler (model 1010, General Oceanics, Inc., USA) equipped with messengers to close the sampler bottles and suspended on a Kevlar rope.

Samples for the DIC, TA, salinity, and  $\delta^{18}\text{O}$  analyses were stored at room temperature in the dark until analysis. Samples for chl.*a* measurements were immediately filtered through a 25-mm-diameter Whatman GF/F filter. Chlorophyll pigment on the filters was then extracted with *N,N*-dimethylformamide (Suzuki and Ishimaru, 1990) for more than 24 h, and the extract was stored between -15 and -20°C until analysis.

## Sample analyses

Seawater DIC was determined by coulometry (Johnson et al., 1985, Johnson et al., 1992) using a hand-made  $\text{CO}_2$  extraction system (Ono et al., 1998) and a coulometer (CM5012, UIC, Inc.,

Binghamton, NY, USA). TA of seawater was determined by titration (Dickson et al., 2007) with a TA analyzer (ATT-05, Kimoto Electric Co., Ltd., Japan). Both DIC and TA measurements were calibrated against reference seawater materials (Batch AO and AP; KANSO Technos Co., Ltd., Osaka, Japan) traceable to the certified reference material distributed by Prof. A. G. Dickson (Scripps Institution of Oceanography, La Jolla, CA, USA). The standard deviations of the DIC and TA measurements, calculated from the results for 10 subsamples of the reference water with DIC = 1987.1  $\mu\text{mol kg}^{-1}$  and TA = 2257.6  $\mu\text{mol kg}^{-1}$ , were <2.0  $\mu\text{mol kg}^{-1}$  and 2.0  $\mu\text{mol kg}^{-1}$ , respectively. The seawater  $p\text{CO}_2$  was computed from DIC and TA using the program CO2SYS, version 02.05 (Orr et al., 2018). For this calculation, we used the carbonic acid dissociation constants ( $K_1$  and  $K_2$ ) of Mehrbach et al. (1973) as revised by Dickson and Millero (1987) and the  $K_{\text{HSO}_4}$  value determined by Dickson (1990).

The seawater salinity was determined with a salinometer (AUTOSAL 8400B, Guildline Instruments, USA). The instrumental accuracy < 0.002 psu. The seawater  $\delta^{18}\text{O}$  was determined with a mass spectrometer (DELTA plus, Finnigan MAT, San Jose, CA, USA) by the equilibration method. The  $\delta^{18}\text{O}$  in permil (‰) was calculated using the  $^{18}\text{O}:^{16}\text{O}$  ratio of standard mean ocean water (SMOW) as the standard. The standard deviation of  $\delta^{18}\text{O}$ , calculated from 10 subsamples of reference water with a  $\delta^{18}\text{O} = +0.241\text{‰}$ , was 0.026‰.

Chl.*a* was determined with a fluorometer (Model 10AU, Turner Designs, Inc., Sunnyvale, CA, USA) by the method of Parsons et al. (1984). Standards (0–150  $\mu\text{g L}^{-1}$  chl.*a*) prepared from a liquid chl.*a* standard (Wako Pure Chemical Industries, Ltd., Osaka, Japan) by stepwise dilution with *N,N*-dimethylformamide were used to calibrate the fluorometer before chl.*a* measurement.

## Calculation of the sea–air $\text{CO}_2$ flux

The sea–air  $\text{CO}_2$  flux was calculated as,

$$F_{\text{sea-air}} = k \cdot \alpha \cdot \Delta p\text{CO}_2 \quad (1)$$

where  $k$  is gas transfer velocity (Wanninkhof et al., 2013),  $\alpha$  is  $\text{CO}_2$  solubility (Weiss, 1974), and  $\Delta p\text{CO}_2$  is the difference in  $p\text{CO}_2$  between the sea surface and the atmosphere. A negative flux indicates absorption of atmospheric  $\text{CO}_2$  by the ocean. The gas transfer velocity was computed by using the mean ( $\pm$  standard deviation) wind speed ( $= 2.9 \pm 2.1 \text{ m s}^{-1}$ ) during the observed month recorded at Qaanaaq weather station (<https://www.timeanddate.com/weather/Greenland/qaanaaq/historic>). Atmospheric  $p\text{CO}_2$  ( $399 \pm 3 \text{ } \mu\text{atm}$ ) was calculated by using the atmospheric  $\text{CO}_2$  concentration ( $= 402 \pm 3 \text{ ppm}$ ) measured at Summit, Greenland (<https://www.esrl.noaa.gov/gmd/dv/iadv/>), the barometric pressure, and saturated water vapor pressure (Weiss and Price, 1980).

## Fractions of glacial and sea ice meltwaters and Arctic water in the fjord

The waters in Bowdoin Fjord were composed mainly of glacial and sea ice meltwaters and Arctic water (Kanna et al., 2018), hereafter referred to as polar water. We calculated the distributions of these three components in Bowdoin Fjord using the following equations (Østlund and Hut, 1984).

$$F_{gm} + F_{sim} + F_{pw} = 1 \quad (2)$$

$$F_{gm} \cdot S_{gm} + F_{sim} \cdot S_{sim} + F_{pw} \cdot S_{pw} = S_{obs} \quad (3)$$

$$F_{gm} \cdot \delta_{gm} + F_{sim} \cdot \delta_{sim} + F_{pw} \cdot \delta_{pw} = \delta_{obs} \quad (4)$$

$F$  represents the fraction of each component in the fjord, and  $S$  and  $\delta$  represent salinity and  $\delta^{18}\text{O}$ , respectively. The subscripts “gm”, “sim”, “pw”, and “obs” represent glacial meltwater, sea ice meltwater, polar water, and observed values. The endmember values of each component are from Kanna et al. (2018). Figure 2 shows the relationship between salinity and  $\delta^{18}\text{O}$  for all samples collected in the fjord and endmember values of each component.

## Results

### Distributions of salinity, temperature, DIC, TA, $p\text{CO}_2$ , chl.*a*, and $\delta^{18}\text{O}$ in surface waters of the fjord

We examined the distributions of salinity, temperature, DIC, TA,  $p\text{CO}_2$ , chl.*a*, and  $\delta^{18}\text{O}$  in the surface water relative to distance from the calving front of Bowdoin Glacier (Figure 3). Except in the plume, salinity near the calving front of Bowdoin Glacier was as low as 3.0 psu (Figure 3A), and it increased with distance from the glacier to a maximum of 30.5 psu. Temperature showed no

relationship with distance from Bowdoin Glacier; the minimum temperature was about  $+3^\circ\text{C}$ , and the maximum was about  $+6^\circ\text{C}$  (Figure 3B). The distributions of DIC and TA were similar to that of salinity; values were low near Bowdoin Glacier and increased with distance from the glacier (Figures 3C, D).  $p\text{CO}_2$  calculated from DIC and TA was 200  $\mu\text{atm}$  or less at all sampling points except in the plume, where it was substantially lower than the atmospheric value of  $399 \pm 3 \mu\text{atm}$  (Figure 3E). Chl.*a* was usually low near the calving front of Bowdoin Glacier, but it was locally markedly high ( $8.0 \mu\text{g L}^{-1}$ ) (Figure 3F). Furthermore, chl.*a* was as high as  $3.7 \mu\text{g L}^{-1}$  even at a distance of 12–15 km from the glacier. The distribution of  $\delta^{18}\text{O}$  was similar to that of salinity, with a maximum of  $-2.0\text{‰}$  and a minimum of  $-21.4\text{‰}$  (Figure 3G). In the plume, salinity, DIC, TA,  $p\text{CO}_2$ , and  $\delta^{18}\text{O}$  were high relative to their values at sampling points outside of the plume. The sea–air  $\text{CO}_2$  flux calculated with Equation 1 was negative everywhere ( $\text{CO}_2$  sink for atmosphere); it ranged from  $-6.5$  to  $-2.1 \text{ mmol m}^{-2} \text{ d}^{-1}$ , and the mean  $\pm$  standard deviation was  $-4.9 \pm 0.7 \text{ mmol m}^{-2} \text{ d}^{-1}$ .

Both DIC and TA showed strong linear relationships with salinity ( $S$ ): Regression line equations were  $\text{DIC} = 54.9S + 167.5$  ( $r^2 = 0.99$ ) in both 2016 and 2017,  $\text{DIC} = 54.2S + 174.9$  ( $r^2 = 0.99$ ) in 2016,  $\text{DIC} = 55.3S + 166.8$  ( $r^2 = 0.99$ ) in 2017, and  $\text{TA} = 63.7S + 105.0$  ( $r^2 = 0.99$ ) in both 2016 and 2017,  $\text{TA} = 64.1S + 102.9$  ( $r^2 = 0.99$ ) in 2016, and  $\text{TA} = 64.8S + 69.1$  ( $r^2 = 0.99$ ) in 2017 (Figures 4A, B).

### Fractions of glacial and sea ice meltwaters and arctic water in the fjord

Figure 5 shows the distribution of the fraction for each component. In Bowdoin Fjord,  $F_{gm}$  was highest, up to 94%, near

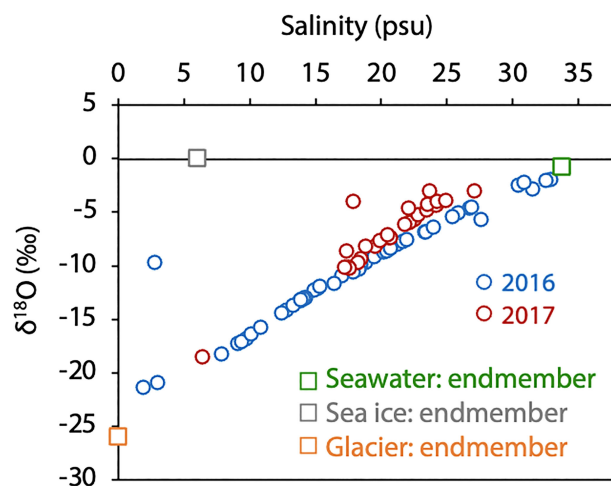


FIGURE 2  
Relationship between  $\delta^{18}\text{O}$  and salinity for surface water and each endmember.

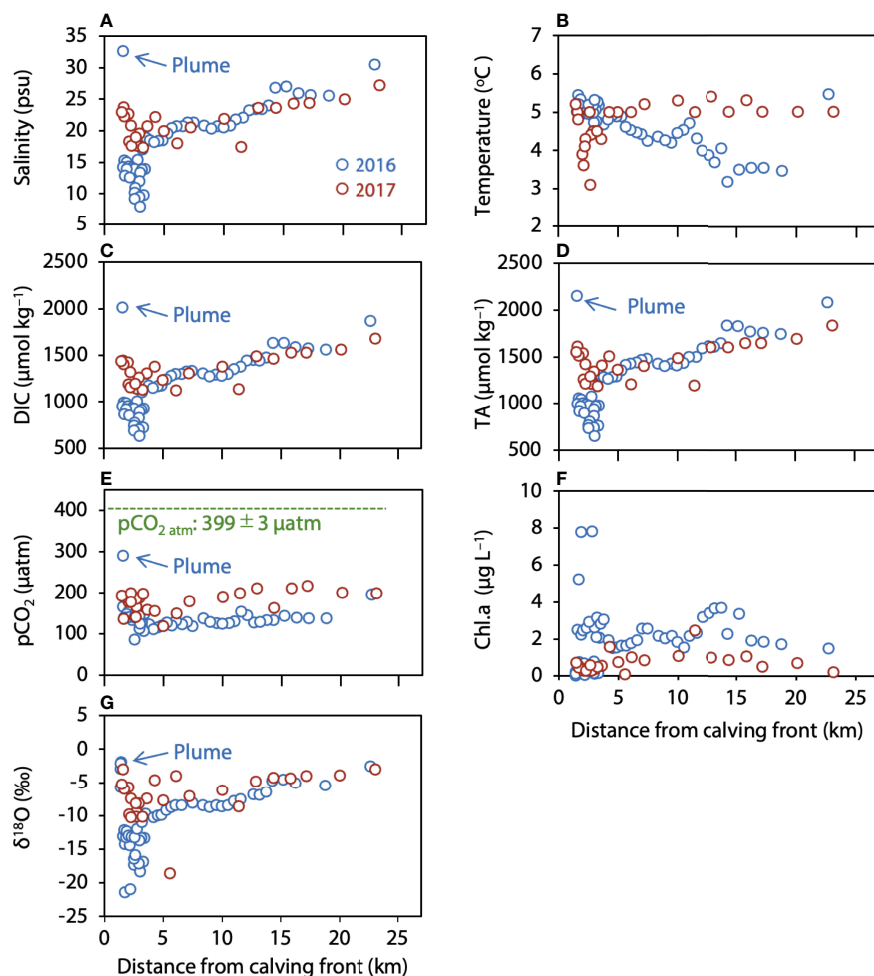


FIGURE 3

Distribution of (A) salinity, (B) temperature, (C) DIC, (D) TA, (E)  $p\text{CO}_2$ , (F) chl.a, and (G)  $\delta^{18}\text{O}$  in surface water in relation to distance from the calving front.

the calving front of Bowdoin Glacier and decreased with distance from the glacier, whereas  $F_{\text{pw}}$  increased with distance from the glacier.  $F_{\text{sim}}$  was low, generally less than 10%, although it reached 14.2% at one point.

## Discussion

### Changes of $p\text{CO}_2$ caused by the dilution effect

The inflow of glacial meltwater was greater closer to the calving front of Bowdoin Glacier (Figures 3, 5). As a result, the salinity of the seawater was decreased close to the front (Figure 3A), and DIC and TA were decreased (Figures 3C, D), by the input of glacial meltwater although glacial meltwater contained DIC and TA because DIC-salinity and TA-salinity

plots exhibit remarkable intercepts at zero salinity (Figures 4A, B).

Here, to evaluate the potential effect in  $p\text{CO}_2$  caused by the decrease in salinity resulting from the input of the freshwater from the melting glacier, the relationship between observed  $p\text{CO}_2$  ( $p\text{CO}_{2\text{ obs}}$ ) and salinity was indicated in Figure 6.  $p\text{CO}_{2\text{ obs}}$  decreased as the salinity decreased. However, when salinity was low (e.g.,  $S < 10$  psu), there was limited  $p\text{CO}_{2\text{ obs}}$  plots (data) (Figure 6) because it was difficult to obtain low salinity samples near the calving front due to dangerous and logistical reasons. In addition, glacier meltwater from Bowdoin Glacier is released from the glacier bed to the bottom of the fjord (Kanna et al., 2018). Therefore, technically, it was difficult to obtain samples to show the  $p\text{CO}_{2\text{ obs}}$  for low salinity water.

Therefore, to indicate  $p\text{CO}_2$  dynamics as a function of the salinity at low salinity water, we calculated  $p\text{CO}_2$  based on the linearities of the DIC and TA with salinity (Figures 4A, B).

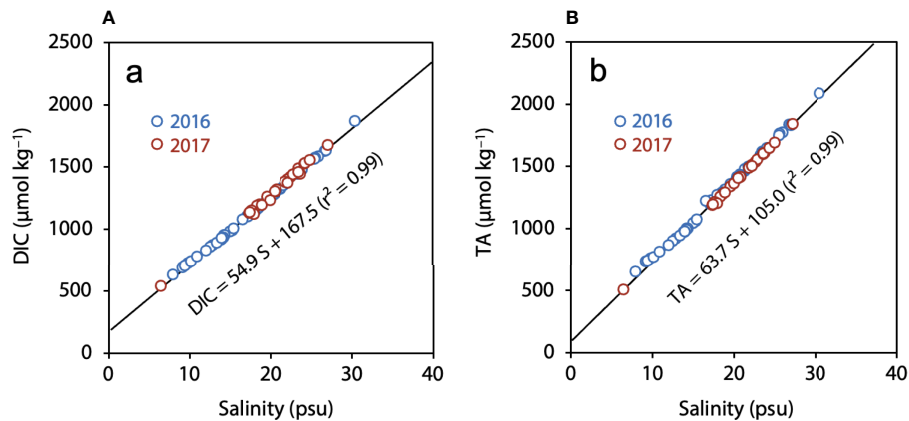


FIGURE 4  
Relationships between (A) DIC, (B) TA and salinity.

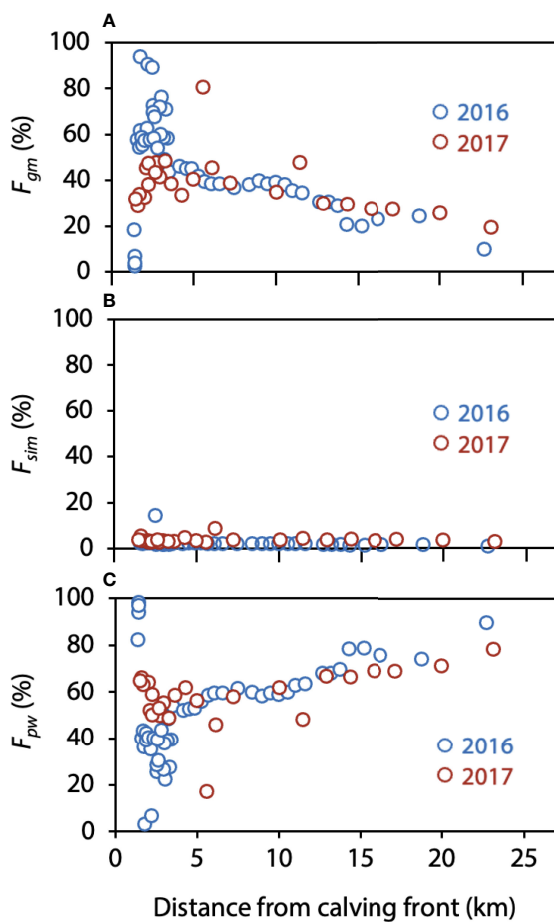


FIGURE 5  
Distributions of the (A) glacial meltwater fraction ( $F_{gm}$ ), (B) sea ice meltwater fraction ( $F_{sim}$ ), and (C) polar water fraction ( $F_{pwr}$ ) in relation to the calving front.

Values of DIC and TA at the any salinity, obtained by using these linear equations ( $DIC = 54.9S + 167.5$  and  $TA = 63.7S + 105.0$  in Figure 4), were decided. Then, we calculated  $pCO_2$  ( $pCO_2_{cal}$ ) using DIC and TA at any salinity. For this calculation, temperature was fixed at  $+5^\circ C$ , which is the surface water near the calving front (Figure 3B) to isolate the effects of DIC and TA changes due to salinity changes on  $pCO_2$ .  $pCO_2_{cal}$  (blue line in Figure 6) decreased as the salinity decreased when salinity was relatively high (e.g.,  $S > 10$  psu). Comparison of  $pCO_2_{cal}$  with  $pCO_2_{obs}$  indicated that variations of  $pCO_2_{cal}$  and  $pCO_2_{obs}$  were similar with respect to the salinity. These results suggested that  $pCO_2_{obs}$  could be explained by the dilution effect as a function of the salinity.

When salinity was low (e.g.,  $S < 10$  psu),  $pCO_2_{cal}$  was substantially higher than the range of  $pCO_2_{obs}$  (60–170  $\mu atm$ ). Because the glacial meltwater contained land-derived substances as indicated that DIC-salinity and TA-salinity plots exhibit remarkable intercepts at zero salinity (Figures 4A, B). Therefore, we expected that  $pCO_2$  at low salinity would be affected by the land-derived substances. In the next section, we will examine the effect of land-derived substances on the  $pCO_2$  by using the relationship between salinity normalized DIC and TA.

## 4.2 Changes of carbonate chemistry due to dissolution of carbonate minerals, decomposition of organic matter, and biological productivity

The positive intercepts of the regression lines fitted to the relationships between DIC and TA and salinity (Figures 4A, B) indicate that the glacial meltwater (unmixed with seawater) contained land-derived substances. To explain the high  $pCO_2_{cal}$  at low salinity, we evaluated effects of land-derived substances

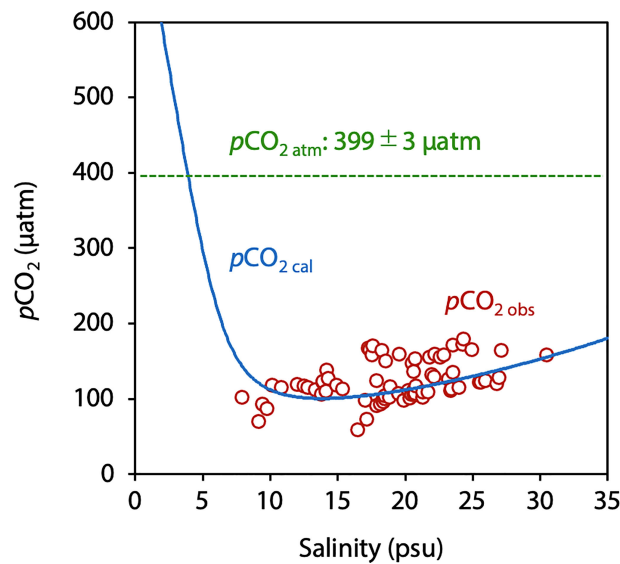


FIGURE 6  
Relationship between  $p\text{CO}_2_{\text{obs}}$  or  $p\text{CO}_2_{\text{cal}}$  and salinity.

on carbonate chemistry by using the relationship between DIC and TA.

To correct for the influences dilution that change DIC and TA proportionally with salinity, DIC and TA were normalized to account for the addition of DIC and TA by freshwater input following Friis et al. (2003) as follows:

$$n\text{DIC} = (\text{DIC}_{\text{obs}} - \text{DIC}_{S=0}) \cdot 34.3/S_{\text{obs}} + \text{DIC}_{S=0} \quad (5)$$

$$n\text{TA} = (\text{TA}_{\text{obs}} - \text{TA}_{S=0}) \cdot 34.3/S_{\text{obs}} + \text{TA}_{S=0} \quad (6)$$

where “nDIC” and “nTA” indicate the salinity normalized DIC and TA. “ $\text{DIC}_{\text{obs}}$ ”, “ $S_{\text{obs}}$ ”, and “ $\text{TA}_{\text{obs}}$ ” indicate the observed values of DIC, salinity, and TA, respectively, at each sampling point. “ $\text{DIC}_{S=0}$ ” and “ $\text{TA}_{S=0}$ ” indicate DIC and TA at  $S = 0$  psu. In this study, we used intercept values of 167.5 for  $\text{DIC}_{S=0}$  and 105.0 for  $\text{TA}_{S=0}$  (Figures 4A, B). “34.3” indicates the salinity of the polar water.

We next plotted nTA against nDIC for all sampling points (Figure 7). We divided the data into two groups: data from sea areas near the glaciers, which were strongly affected by the glacier meltwater (e.g.,  $S < 15$  psu) (red circles) and data from other areas less affected by glacier meltwater (e.g.,  $S > 15$  psu) (blue circles). The expected changes in nDIC and nTA due to photosynthesis and organic matter decomposition ( $\text{slope} = 2.0$ ), based on the Redfield ratio (C:N:P = 106:16:1) ( $\text{slope} = -0.14$ ), the dissolution or precipitation of calcium carbonate, and the exchange of  $\text{CO}_2$  between the atmosphere and the ocean ( $\text{slope} = 0$ ) (Zeebe and Wolf-Gladrow, 2001) were shown in the inset in Figure 7.

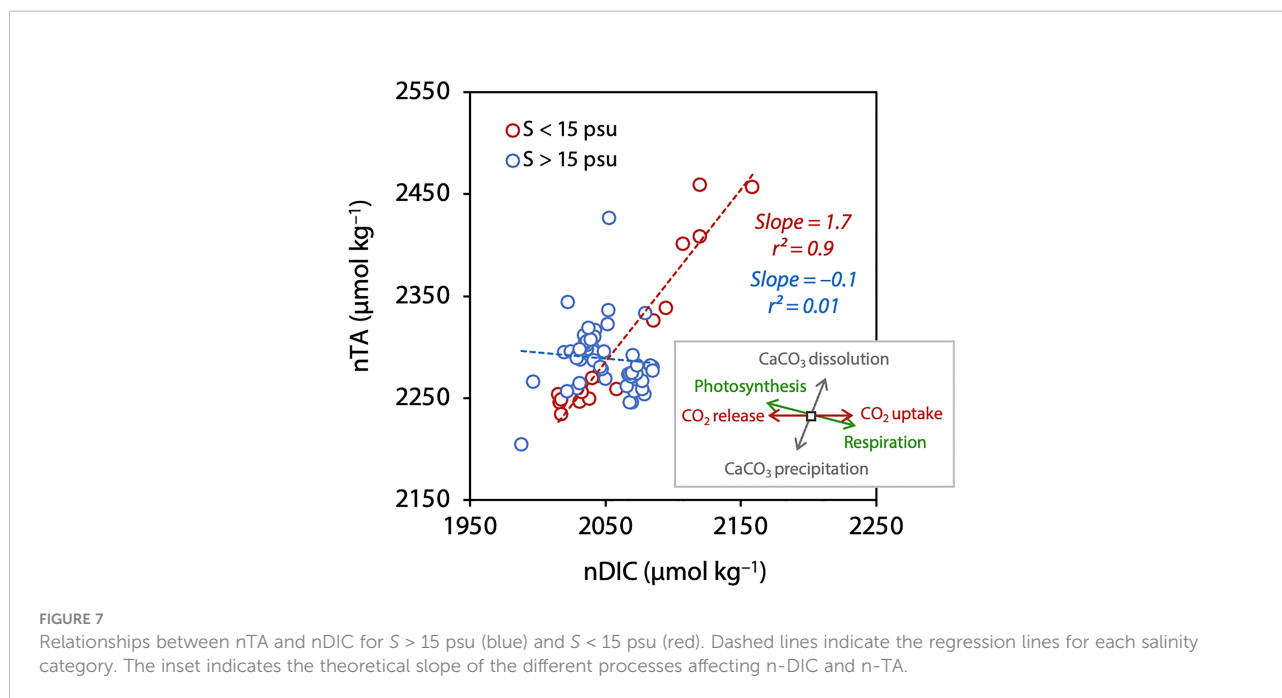
Data for  $S > 15$  psu (blue) was relatively narrow range ( $2047 \pm 22 \mu\text{mol kg}^{-1}$  for nDIC and  $2289 \pm 31 \mu\text{mol kg}^{-1}$  for nTA) with respect to those for  $S < 15$  psu (red) (Figure 7). Data for  $S < 15$  psu ranged widely from 2015 to 2158  $\mu\text{mol kg}^{-1}$  for nDIC and 2233 to

2458  $\mu\text{mol kg}^{-1}$  for nTA with respect to those of  $S > 15$  psu. In addition, data for  $S < 15$  psu deviated from the data for  $S > 15$  psu to the higher nDIC and nTA (upper right side). Furthermore, the relationship between nDIC and nTA for  $S < 15$  psu indicated high correlation ( $r^2 = 0.9$ ) with slope of 1.7. These results suggest that nDIC and nTA were changed by the mixing effects of dissolution of minerals such as calcium carbonate, the decomposition of organic matter (respiration), and absorption of  $\text{CO}_2$  from the atmosphere ( $\text{CO}_2$  uptake).

To understand dominant processes affecting nDIC and nTA variations, we first examined the change in nDIC (nTA does not change) due to the absorption of  $\text{CO}_2$  from the atmosphere. In this study, we calculated the  $\text{CO}_2$  flux between ocean and atmosphere to be  $-4.9 \pm 0.7 \text{ mmol m}^{-2} \text{ d}^{-1}$  during the 15 days from mid-July, when sea ice melting started, to the end of our observation period (beginning of August) (see section 3.1). Given this flux, the increase in nDIC at the surface (e.g., 0–10 m depth) due to  $\text{CO}_2$  absorption from the atmosphere was calculated to be  $7 \mu\text{mol kg}^{-1}$ . This value is very small compared to the observed nDIC increases for  $S < 15$  psu (Figure 7;  $>140 \mu\text{mol kg}^{-1}$  increase). Thus, we inferred that the effect on the nDIC increase of the exchange of  $\text{CO}_2$  between the atmosphere and ocean was negligible.

How does the dissolution of minerals affect nDIC and nTA near the calving front? As shown by the formulas for carbonate mineral dissolution ( $\text{CaCO}_3 + \text{CO}_2(\text{aq}) + \text{H}_2\text{O} \rightarrow \text{Ca}^{2+} + 2\text{HCO}_3^-$ ) and silicate mineral dissolution ( $\text{CaAl}_2\text{Si}_2\text{O}_8 + 2\text{CO}_2(\text{aq}) + 2\text{H}_2\text{O} \rightarrow \text{Ca}^{2+} + 2\text{HCO}_3^-(\text{aq}) + \text{H}_2\text{Al}_2\text{Si}_2\text{O}_8$ ), the dissolution of both carbonate and silicate minerals would cause nDIC and nTA to increase in the ratio of 1:2 ( $\text{slope} =$





2.0). Glacial meltwater flowing into Bowdoin Fjord also contains organic particles (Kanna et al., 2018). When these organic particles are remineralized by bacterial activity (respiration), nDIC increases and nTA decreases according to the Redfield ratio (C:N:P = 106:16:1). The dissolution of minerals and the decomposition of organic matter occur at the same time. Therefore, nDIC and nTA affected by glacial meltwater should plot between the theoretical lines for these processes.

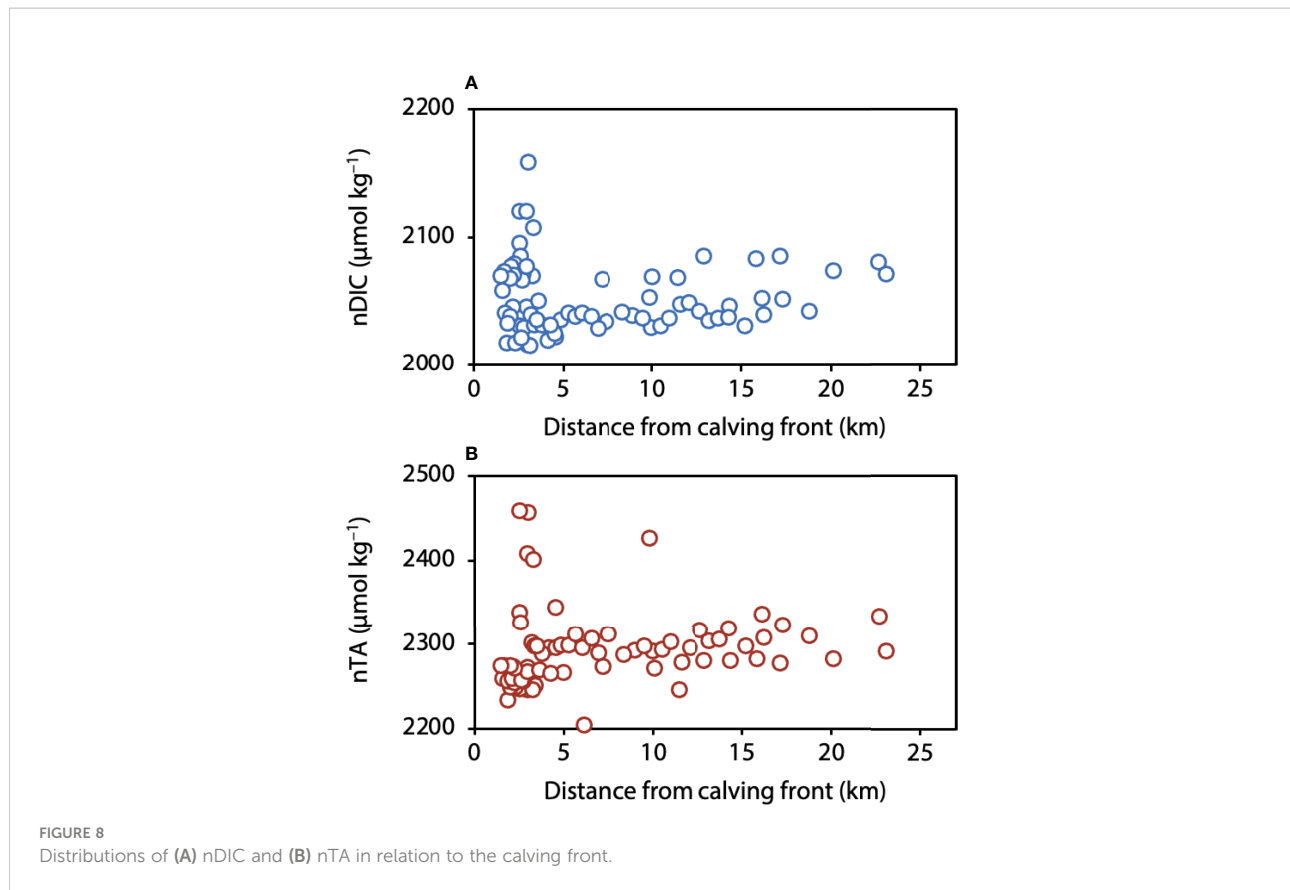
In this discussion, we have assumed that the dissolution of carbonate minerals and the decomposition of organic matter occur *in situ* (i.e., in the fjord waters), but it is possible for these processes to affect the chemistry of the glacial meltwater before it flows into the fjord. Near the calving front of Bowdoin Glacier, where the influence of glacial meltwater is large (Figure 5A), nDIC and nTA were higher than nDIC and nTA of other area (Figures 8A, B). Therefore, DIC and TA components were added to the fjord water, either as a result of the dissolution of minerals such as calcium carbonate and the decomposition of organic matter occurring within the fjord waters, as described above, or as a result of mineral dissolution and organic matter decomposition occurring in the glacial meltwater before it flowed into the fjord. Podolskiy et al. (2021) estimated residence time near the calving front of the glacier to be about several days based on the time series of the surface water temperature. Therefore, we inferred that DIC and TA components were added by the glacial meltwater affected by the dissolution of minerals such as calcium carbonate and the decomposition of organic matter before it flowed into the fjord. This discussion was supported by the results that DIC-salinity and TA-salinity plots exhibit high correlation coefficient ( $r^2 = 0.99$ ) and the remarkable intercepts at zero salinity (Figures 4A, B). For the biological productivity, the

effect of photosynthesis on the carbonate chemistry would be minimum because the short residence time of water and the low temperature water near the calving front have restrained primary production.

Given these impacts on nDIC and nTA, how does the dissolution of minerals and the decomposition of organic matter in the glacial meltwater affect  $p\text{CO}_2$ ? The dissolution formulas for minerals given above show that dissolution works to reduce  $p\text{CO}_2$  of the seawater because it consumes  $\text{CO}_2$  (St Pierre et al., 2019). In contrast, when organic particles are decomposed,  $p\text{CO}_2$  of the seawater increases. Based on our  $p\text{CO}_2$  distribution (Figure 6) and the relationship between nDIC and nTA suggested that the dilution effect by freshwater was dominant in relatively higher salinity (e.g.,  $S > 15$  psu) site away from the glacier while for the lower salinity (e.g.,  $S < 15$  psu) site near the calving front, the land-derived high  $p\text{CO}_2$  freshwater affected mainly by the remineralization of the organic matter by bacterial activity was supplied to the fjord. Glacial meltwater flowing into the Bowdoin Fjord contains organic particles (Kanna et al., 2018). Therefore, we suggested that in our study area, the remineralization process was dominated and  $p\text{CO}_2$  near the calving front was increased.

## 5 Conclusion

Water was sampled in Bowdoin Fjord, northwestern Greenland, to examine the effects of glacier meltwater supply on the  $\text{CO}_2$  cycle within the fjord. The inflow of glacial meltwater was greater closer to the calving front of Bowdoin Glacier. As a result, the salinity of the seawater decreased near the ice front, and DIC and TA were decreased, by the input of glacial meltwater. The



$p\text{CO}_2$  variation suggested that the dilution effect was dominant in relatively higher salinity (e.g.,  $S > 15$  psu) site away from the glacier. However, for the lower salinity (e.g.,  $S < 15$  psu) site near the calving front,  $p\text{CO}_2$  was high due to the supply of the water affected by the decomposition of organic matter before it flowed into the fjord. Because the actual meltwaters from the glacier especially flowing *via* the land contained the terrestrial materials, inorganic carbon dynamics in such coastal fjord waters requires consideration of not only the dilution effect of glacial meltwater but also the biogeochemical modification by the land-derived substances supplied with freshwater.

Our results present facilitate understanding of the effects of glacial meltwater on carbon dynamics in seawater and subsequent prediction of future changes in the carbonate chemistry of the fjord, and thus the amount of  $\text{CO}_2$  absorbed from the atmosphere because the accelerated melting of glacier and ice shelves in recent years (e.g., Pritchard et al., 2012; Rignot et al., 2019) has provided large amounts of freshwater to the coastal areas and high productivity was observed (e.g., Meire et al., 2015; Arrigo et al., 2017). In addition to the freshwater, our results indicated that materials were supplied to the coastal areas, which would be modified the carbonate chemistry in the water, and thereby  $\text{CO}_2$  flux between ocean and atmosphere.

Further investigations are needed for understanding the materials transport and the effects on the carbonate chemistry and gas flux process in the future.

## Data availability statement

The original contributions presented in the study are included in the article/Supplementary Material and the data repository of the National Institute of Polar Research, Tokyo, Japan (<https://doi.org/10.17592/001.2022070101>). Further inquiries can be directed to the corresponding author.

## Author contributions

The original collectors of field data for this synthesis are DN, NK, YF, and SS. TH performed the data reevaluation and wrote the paper with contributions from all coauthors. All authors contributed to the article and approved the submitted version.

## Funding

This work was supported by grants from the Japan Society for the Promotion of Science (JSPS) (#17H04715, #20H04345) and the Japanese Ministry of Education, Culture, Sports, Science and Technology (MEXT) through the Arctic research project, Arctic Challenge for Sustainability (ArCS) (JPMXD1300000000) and ArCS-II (JPMXD1420318865), and the Joint Research Program of the Institute of Low Temperature Science, Hokkaido University.

## Acknowledgments

We thank all of the people working in the field during the 2016 and 2017 field campaigns in Qaanaaq. Special thanks are due to S. Daorana, T. Oshima, and K. Peterson for providing logistical support in Qaanaaq. We are also grateful to D. Sakakibara, Y. Ohashi, S. Yunoki for assistance with the field and laboratory tasks. The Landsat image used for Figure 1 was downloaded from the U.S. Geological Survey Earth Explorer.

## References

- Östlund, H. G., and Hut, G. (1984). Arctic Ocean water mass balance from isotope data. *J. Geophysical. Res.* 89 (C4), 6373–6381. doi: 10.1029/JC089iC04p06373
- Arrigo, K. R., van Dijken, G. L., Castelao, R. M., Luo, H., Rennermalm, Å.K., Tedesco, M., et al. (2017). Melting glaciers stimulate large summer phytoplankton blooms in southwest Greenland waters. *Geophysical. Res. Lett.* 44, 6278–6285. doi: 10.1002/2017GL073583
- Bates, N. R., and Mathis, J. T. (2009). The Arctic ocean marine carbon cycle: evaluation of air-sea CO<sub>2</sub> exchanges, ocean acidification impacts and potential feedbacks. *Biogeosciences* 6, 2433–2459. doi: 10.5194/bg-6-2433-2009
- Björk, A. A., Kruse, L. M., and Michaelsen, P. B. (2015). Getting greenland's glaciers right—a new data set of all official greenlandic glacier names. *Cryosphere*. 9 (6), 2215–2218. doi: 10.5194/tc-9-2215-2015
- Carr, J. R., Stokes, C. R., and Vieli, A. (2017). Threefold increase in marine terminating outlet glacier retreat rates across the Atlantic Arctic 1992–2010. *Ann. Glaciol.* 58, 72–91. doi: 10.1017/aog.2017.3
- Chu, V. W. (2014). Greenland Ice sheet hydrology, a review. *Prog. Phys. Geogr.* 38 (1), 19–54. doi: 10.1177/0309133313507075
- Dickson, A. G. (1990). Standard potential of the reaction: AgCl(s) + 1.2H<sub>2</sub>(g) = ag(s) + HCl(aq), and the standard acidity constant of the ion HSO<sub>4</sub><sup>-</sup> in synthetic sea water from 273.15 to 318.15. *J. Chem. Thermodynamics*. 22, 113–127. doi: 10.1016/0021-9614(90)90074-Z
- Dickson, A. G., and Millero, F. J. (1987). A comparison of the equilibrium constants for the dissociation of carbonic acid in seawater media. *Deep-Sea. Res.* 34, 1733–1743. doi: 10.1016/0198-0149(87)90021-5
- Fransson, A., Chierici, M., Nomura, D., Granskog, M. A., Kristiansen, S., Martma, T., et al. (2015). Effect of glacial drainage water on the CO<sub>2</sub> system and ocean acidification state in an Arctic tidewater-glacier fjord during two contrasting years. *J. Geophysical. Research-Oceans*. 120, 2413–2429. doi: 10.1002/2014JC010320
- Friis, K., Kortzinger, A., and Wallace, D. W. R. (2003). The salinity normalization of marine inorganic carbon chemistry data. *Geophysical. Res. Lett.* 30 (2), 1085. doi: 10.1029/2002GL015898
- Gao, Z., Chen, L., Sun, H., Chen, B., and Cai, W. J. (2012). Distributions and air-sea fluxes of carbon dioxide in the Western Arctic ocean. *Deep-Sea. Res. II*. 81–84, 46–52. doi: 10.1016/j.dsr2.2012.08.021

## Conflict of interest

The authors declare that the research was conducted in the absence of any commercial or financial relationships that could be construed as a potential conflict of interest.

## Publisher's note

All claims expressed in this article are solely those of the authors and do not necessarily represent those of their affiliated organizations, or those of the publisher, the editors and the reviewers. Any product that may be evaluated in this article, or claim that may be made by its manufacturer, is not guaranteed or endorsed by the publisher.

## Supplementary material

The Supplementary Material for this article can be found online at: <https://www.frontiersin.org/articles/10.3389/fmars.2022.873860/full#supplementary-material>

- Johnson, K. M. (1992). *Single-operator multiparameter metabolic analyzer (SOMMA) for total carbon dioxide (CT) with coulometric detection. SOMMA manual 1.0, January 1992* (Upton, NY: Brookhaven National Laboratory), 70 pp. doi: 10.2172/10194787
- Johnson, K. M., King, A. E., and Sieburth, J. M. (1985). Coulometric TCO<sub>2</sub> analyses for marine studies; an introduction. *Mar. Chem.* 16, 61–82. doi: 10.1016/0304-4203(85)90028-3
- Kanna, N., Sugiyama, S., Fukamachi, Y., Nomura, D., and Nishioka, J. (2020). Iron supply by subglacial discharge into a fjord near the front of a marine-terminating glacier in Northwestern Greenland. *Global Biogeochemical. Cycles* 34 (123), 1666–1682. doi: 10.1029/2020GB006567
- Kanna, N., Sugiyama, S., Ohashi, Y., Sakakibara, D., Fukamachi, Y., and Nomura, D. (2018). Upwelling of macronutrients and dissolved inorganic carbon by a subglacial freshwater driven plume in bowdoin fjord, northwestern Greenland. *J. Geophysical. Research-Biogeosciences*. doi: 10.1029/2017JG004248
- Mehrbach, C., Culberson, C. H., Hawley, J. E., and Pytkowicz, R. M. (1973). Measurement of the apparent dissociation constants of carbonic acid in seawater at atmospheric pressure. *Limnology. Oceanography*. 18 (6), 897–907. doi: 10.4319/lo.1973.18.6.0897
- Meire, L., Mortensen, J., Meire, P., Juul-Pedersen, T., Sej, M. K., Rysgaard, S., et al. (2017). Marine-terminating glaciers sustain high productivity in Greenland fjords. *Global Change Biol.* 23 (12), 5344–5357. doi: 10.1111/gcb.13801
- Meire, L., Søgaard, D. H., Mortensen, J., Meysman, F. J. R., Soetaert, K., Arendt, K. E., et al. (2015). Glacial meltwater and primary production are drivers of strong CO<sub>2</sub> uptake in fjord and coastal waters adjacent to the Greenland ice sheet. *Biogeosciences* 12, 2347–2363. doi: 10.5194/bg-12-2347-2015
- Naito, A., Abe, Y., Matsuno, K., Nishizawa, B., Kanna, N., Sugiyama, S., et al. (2019). Surface zooplankton size and taxonomic composition in bowdoin fjord, north-western Greenland: A comparison of ZooScan, OPC and microscopic analyses. *Polar. Sci.* 19, 120–129. doi: 10.1016/j.polar.2019.01.001
- Nienow, P. W., Sole, A. J., Slater, D. A., and Cowton, T. R. (2017). Recent advances in our understanding of the role of meltwater in the Greenland ice sheet system. *Curr. Clim. Change Rep.* 3, 330–344. doi: 10.1007/s40641-017-0083-9
- Nishizawa, B., Kanna, N., Ohashi, Y., Sakakibara, D., Asaji, I., Abe, Y., et al. (2019). Contrasting assemblages of seabirds in the subglacial meltwater plume and oceanic water of bowdoin fjord, northwestern Greenland. *ICES. J. Mar. Sci.* 77 (2), 711–720. doi: 10.1093/icesjms/fsz213
- Ohashi, Y., Aoki, S., Matsumura, Y., Sugiyama, S., Kanna, N., and Sakakibara, D. (2020). Vertical distribution of water mass properties under the influence of

subglacial discharge in bowdoin fjord, northwestern Greenland. *Ocean. Sci.* 16, 545–564. doi: 10.5194/os-16-545-2020

Ono, T., Watanabe, S., Okuda, K., and Fukasawa, M. (1998). Distribution of total carbonate and related properties in the north pacific along 30°N. *J. Geophysical Res.* 103 (C13), 30873–30883. doi: 10.1029/1998jc900018

Orr, J. C., Epitalon, J.-M., Dickson, A. G., and Gattuso, J.-P. (2018). Routine uncertainty propagation for the marine carbon dioxide system. *Mar. Chem.* 207, 84–107. doi: 10.1016/j.marchem.2018.10.006

Parsons, T. R., Takahashi, M., and Hargrave, B. (1984). *Biological Oceanographic Processes (3rd ed.)* (Oxford, UK: Pergamon: ELSEVIER).

Podolskiy, E. A., Kanna, N., and Sugiyama, S. (2021). Co-Seismic eruption and intermittent turbulence of a subglacial discharge plume revealed by continuous subsurface observations in Greenland. *Communication. Earth Environ.* 2 (66), 2–66. doi: 10.1038/s43247-021-00132-8

Pritchard, H., Ligtenberg, S., Fricker, H., Vaughan, D. G., van den Broeke, M. R., and Padman, L. (2012). Antarctic Ice-sheet loss driven by basal melting of ice shelves. *Nature* 484, 502–505. doi: 10.1038/nature10968

Rignot, E., Mouginot, J., Scheuchl, B., van den Broeke, M., van Wessem, M. J., and Morlighem, M. (2019). Four decades of Antarctic ice sheet mass balance from 1979–2017. *Proc. Natl. Acad. Sci.* 116 (4), 1095–1103. doi: 10.1073/pnas.1812883116

Seifert, M., Hoppema, M., Burau, C., Elmer, C., Friedrichs, A., Geuer, J. K., et al. (2019). Influence of glacial meltwater on summer biogeochemical cycles in scoresby sund, East Greenland. *Front. Mar. Sci.* 6. doi: 10.3389/fmars.2019.00412

Sejr, M. K., Krause-Jensen, D., Rysgaard, S., Sorensen, L. L., Christensen, P. B., and Glud, R. N. (2011). Air-sea flux of CO<sub>2</sub> in arctic coastal waters influenced by glacial melt water and sea ice. *Tellus* 63B, 815–822. doi: 10.1111/j.1600-0889.2011.00540x

St Pierre, K. A., St Louis, V. L., Schiff, S. L., Lehnerr, I., Dainard, P. G., Gardner, A. S., et al. (2019). Proglacial freshwaters are significant and previously unrecognized sinks of atmospheric CO<sub>2</sub>. *Proc. Nat. Sci. U.S.A.* 116 (36), 17690–17695. doi: 10.1073/pnas.1904241116

Sugiyama, S., Kanna, N., Sakakibara, D., Ando, T., Asaji, I., Kondo, K., et al. (2021). Rapidly changing glaciers, ocean and coastal environments, and their impact on human society in the qaanaaq region, northwestern Greenland. *Polar. Sci.* 27, 100631. doi: 10.1016/j.polar.2020.100632

Sugiyama, S., Sakakibara, D., Tsutaki, S., Maruyama, M., and Sawagaki, T. (2015). Glacier dynamics near the calving front of bowdoin glacier, northwestern Greenland. *J. Glaciology*. 61, 226. doi: 10.3189/2015JG14J127

Suzuki, R., and Ishimaru, T. (1990). An improved method for the determination of phytoplankton chlorophyll using n, n-dimethylformamide. *J. Oceanography*. 46, 190–194. doi: 10.1007/bf02125580

Tsutaki, S., Sugiyama, S., Sakakibara, D., and Sawagaki, T. (2016). Surface elevation changes during 2007–13 on bowdoin and tugto glaciers, northwestern Greenland. *J. Glaciology*. 62 (236), 1083–1092. doi: 10.1017/jog.2016.106

Wanninkhof, R., Park, G.-H., Takahashi, T., Sweeney, C., Feely, R., Nojiri, Y., et al. (2013). Global ocean carbon uptake: Magnitude, variability and trends. *Biogeosciences* 10 (3), 1983–2000. doi: 10.5194/bg-10-1983-2013

Weiss, R. F. (1974). Carbon dioxide in water and seawater: The solubility of a non-ideal gas. *Mar. Chem.* 2 (3), 203–215. doi: 10.1016/0304-4203(74)90015-2

Weiss, R. F., and Price, B. A. (1980). Nitrous oxide solubility in water and sea water. *Mar. Chem.* 8 (1980), 347–359. doi: 10.1016/0304-4203(80)90024-9

Zeebe, R. E., and Wolf-Gladrow, D. A. (2001). *CO<sub>2</sub> in seawater: Equilibrium, kinetics, isotopes, elsevier oceanography series volume 65* (Amsterdam, the Netherlands: Elsevier).